Supporting Information

Exploring the Spatial Distribution and Transport Behavior of Charge Carriers in a Single Titania Nanowire

Takashi Tachikawa and Tetsuro Majima**

The Institute of Scientific and Industrial Research (SANKEN), Osaka University, Mihogaoka 8-1, Ibaraki, Osaka 567-0047, Japan

Contents

Estimation of the thickness of the space-charge layer of TNW.

The thickness of the space-charge layer can be described by[S1]

$$W = \left[\frac{2\varepsilon\varepsilon_0 V_b}{eN_d} \right]^{1/2},$$

where ε_0 is the permittivity of free space (8.86×10^{-12} Fm^{-1} [S2]), ε is the dielectric constant (48 Fm^{-1} for TiO_2 [S2]), e is the electronic charge unit, N_d is the dopant density (2×10^{18} cm^{-3} [S2]), and V_b is the band bending potential (0.8 V [S3]). The W value has been calculated to be ca. 50 nm, which is comparable to the size of the wires (100 nm in width and 30 nm in height). This estimate implies that the effect of space charge layer is not negligible.

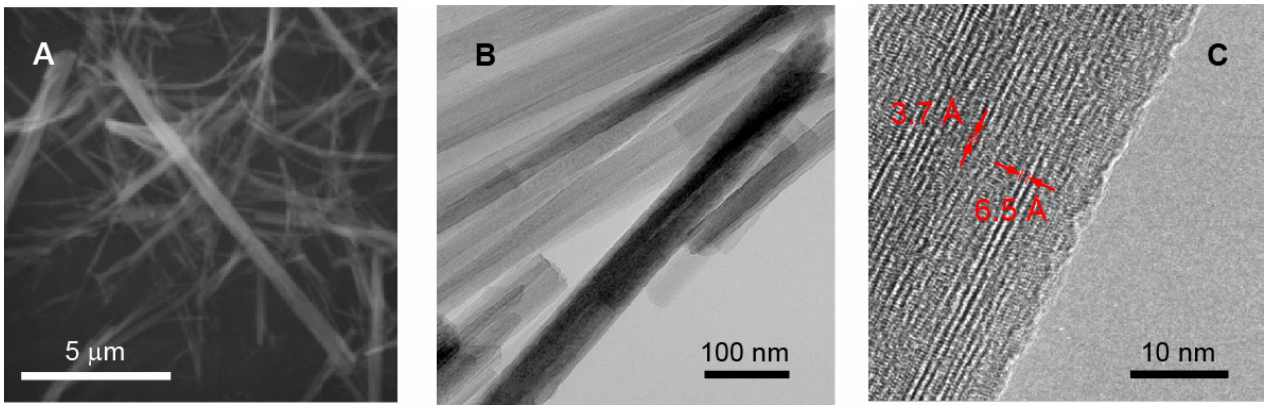

Figure S1. Scanning electron microscope (SEM, Hitachi, S-2250N) (A) and transmission electron microscope (TEM, Hitachi, H-9000, 300 kV) (B and C) images of synthesized TNWs. High-resolution lattice image viewed down the [100] projection (C).

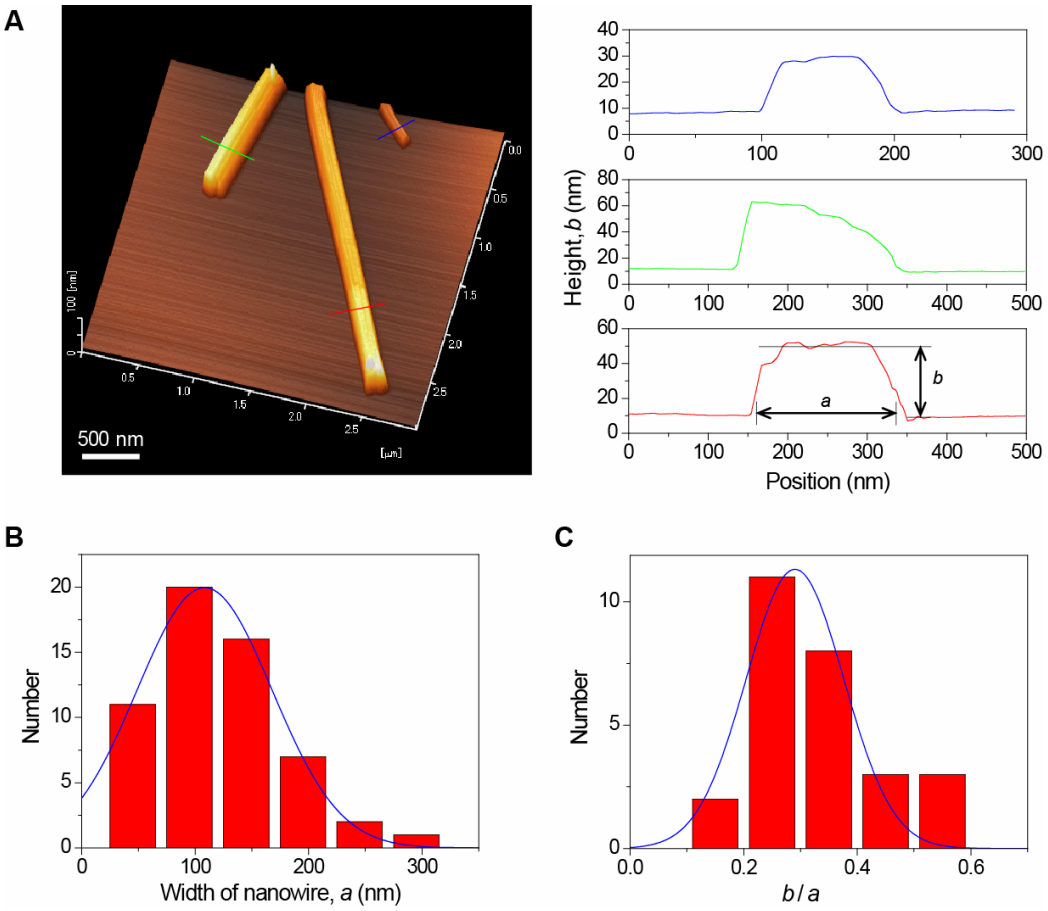

Figure S2. (A) Atomic force microscope (AFM, Seiko Instruments, SPA400-DFM, SI-DF20) image of TNWs spin-coated on a mica surface. Right panels show the cross-sections along the corresponding colored lines (red, green, and blue). Histograms for the wire widths (*a*) (B) and the ratio of *a* to the height (*b*) (C).

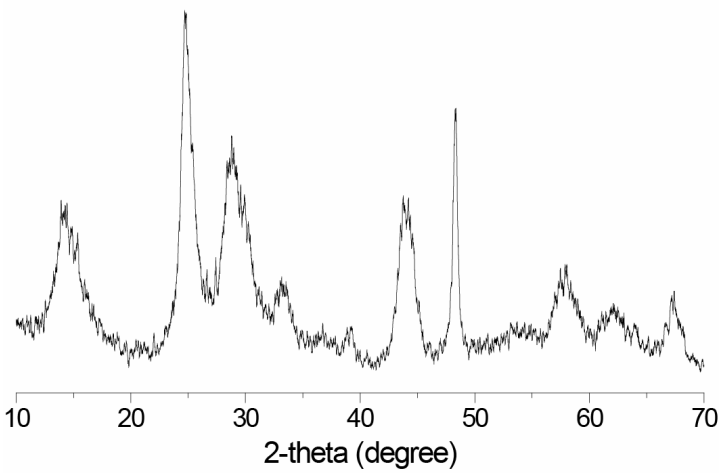

Figure S3. Powder X-ray diffraction (XRD) pattern of synthesized TNWs (Rigaku, RINT2500 XRD spectrometer with Cu Kα radiation). All diffraction peaks could be indexed as TiO_2-B. See ref S4 for peak assignments.

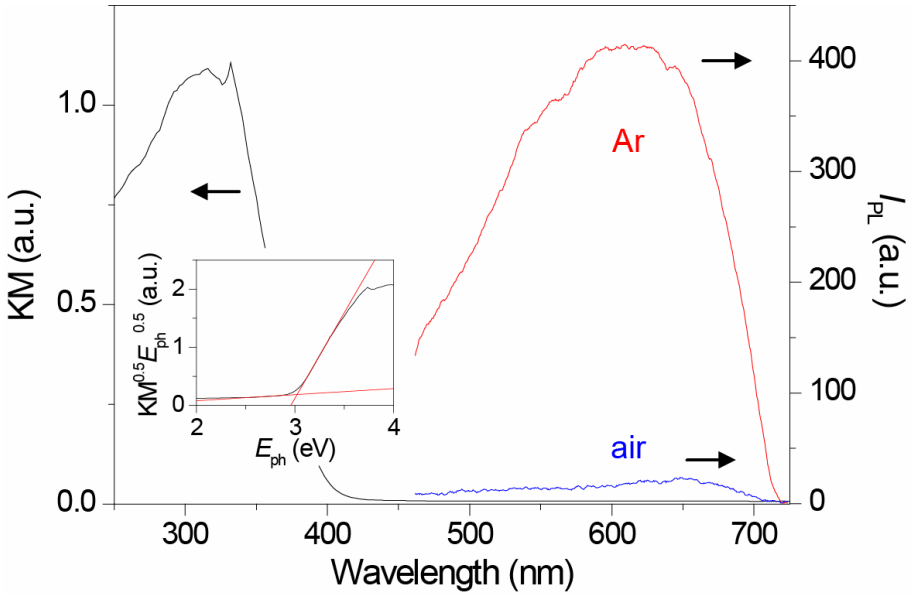

Figure S4. Steady-state UV-visible diffuse reflectance (black) and emission spectra (red and blue) of TNWs at the ensemble level. Inset shows the plot of the square root of the Kubelka-Munk function (KM) versus the photon energy (E_{ph}). The band gap energy (E_g) was estimated to be 3.0 ± 0.1 eV. The emission spectra were measured under the microscope (Olympus IX71, see main text for details) after the 405-nm laser irradiation for 5 min at room temperature. The diffuse reflectance spectrum was measured by UV-visible-near-infrared spectrophotometer (Jasco, V-570) at room temperature.

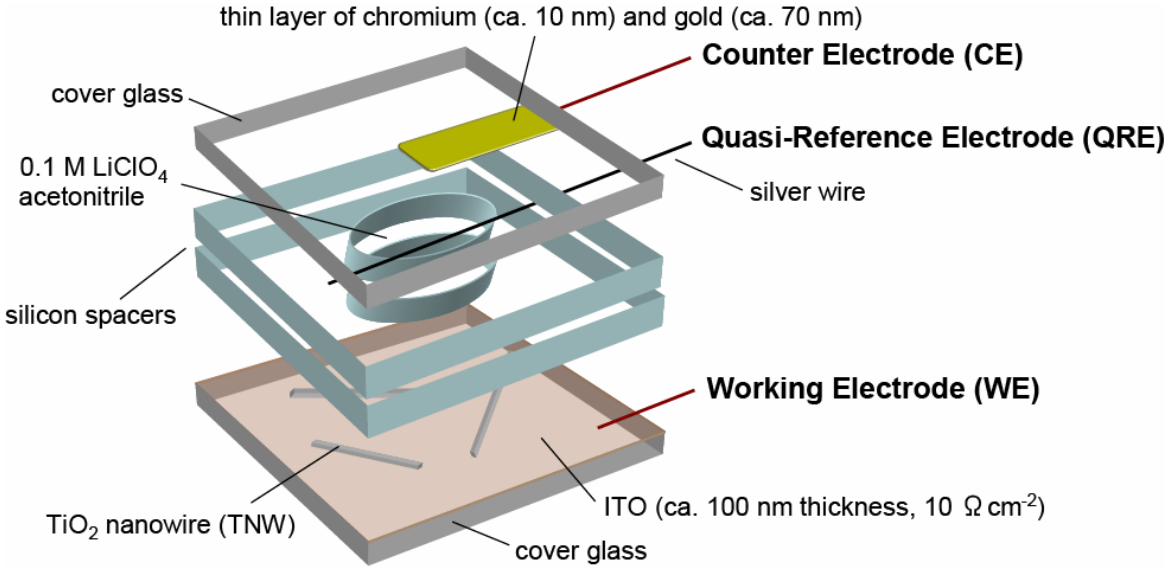

Figure S5. Cell configuration for single-particle electrochemical measurements.

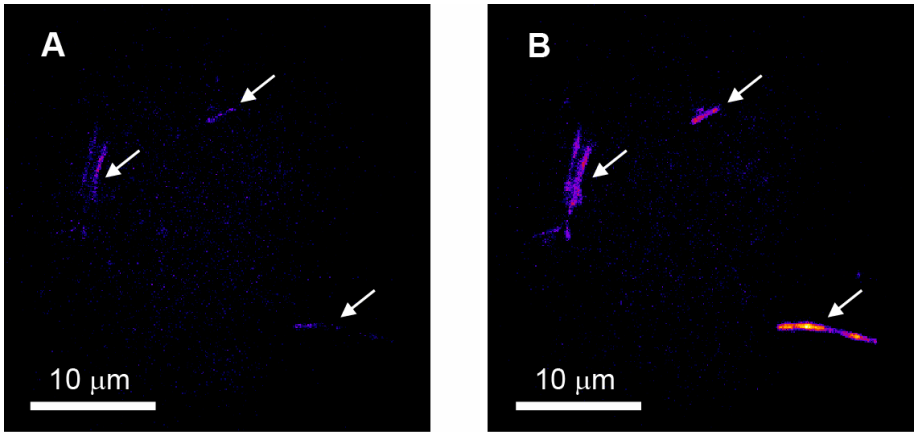

Figure S6. PL images observed for TNWs before (A) and after (B) the photoactivation during 405-nm laser irradiation in an Ar atmosphere.

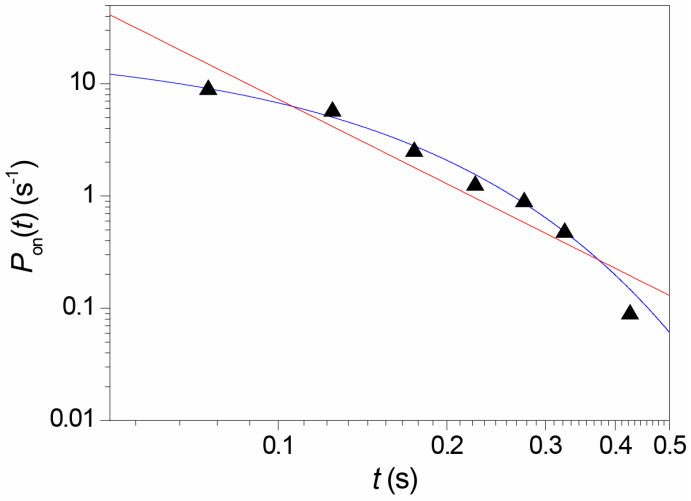

Figure S7. On-time probability density, $P_{on}(t)$,[S5,6] obtained for single TNWs in Ar ([O_2] = 0.2 vol%). The red line indicates the power law fit, $P_{on}(t) = At^{-\alpha_{on}}$, where A is the scaling coefficient and α_{on} is the power law exponent. The α_{on} value was determined to be 2.5 ± 0.1 (R^2 = 0.95), which is much higher than those (1.7-1.9) reported for the single quantum dots[S5] and wires[S7,8] of CdSe. It was also found that the $P_{on}(t)$ is well fitted by a single-exponential decay function (blue line) (R^2 = 0.99).

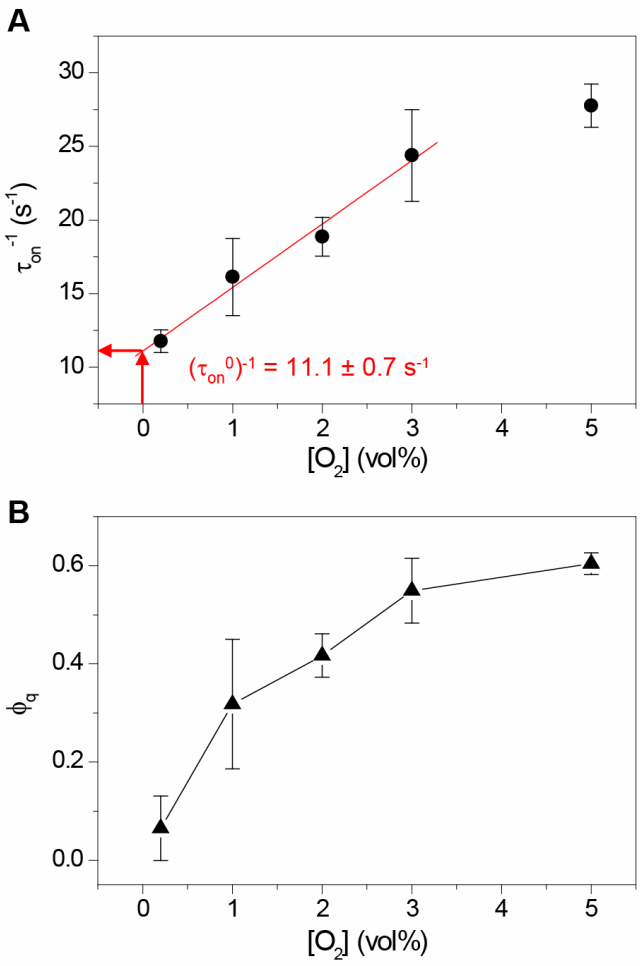

Figure S8. (A) The oxygen concentration dependence of τ_{on}^{-1}. The on-time of the bursts in the absence of oxygen (τ_{on}^{0}) is roughly estimated to be 90 ms from the intercept of the plots (see the red line). (B) The quenching yield of the bursts by oxygen (ϕ_q) as a function of the oxygen concentration in the gas phase, where $\phi_q = 1 - (\tau_{on}/\tau_{on}^{0})$. See ref S9 for a precise formulation.

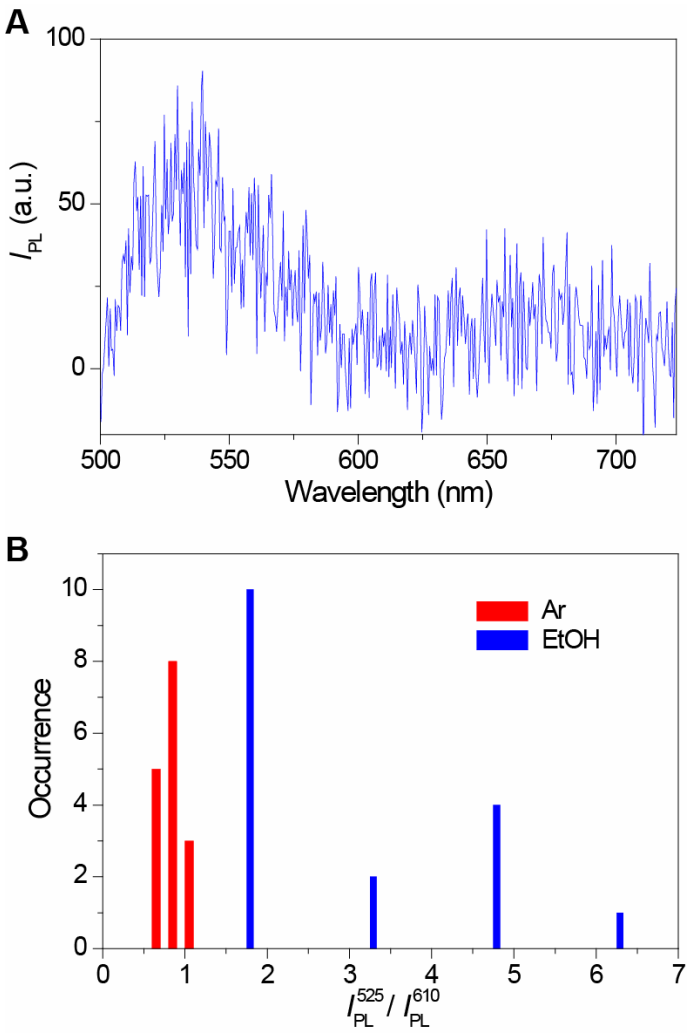

Figure S9. (A) PL spectrum observed for individual TNWs after the 405-nm laser irradiation for 1 min in an Ar-saturated EtOH. (B) Histogram for the intensity ratio of 525 nm to 610 nm of PL spectra obtained in an Ar atmosphere and an Ar-saturated EtOH. McHale et al. concluded that the green PL with a peak around 525 nm is due to the transition between the mobile electrons (those in the conduction band or in shallow bulk traps) and trapped holes.[S10]

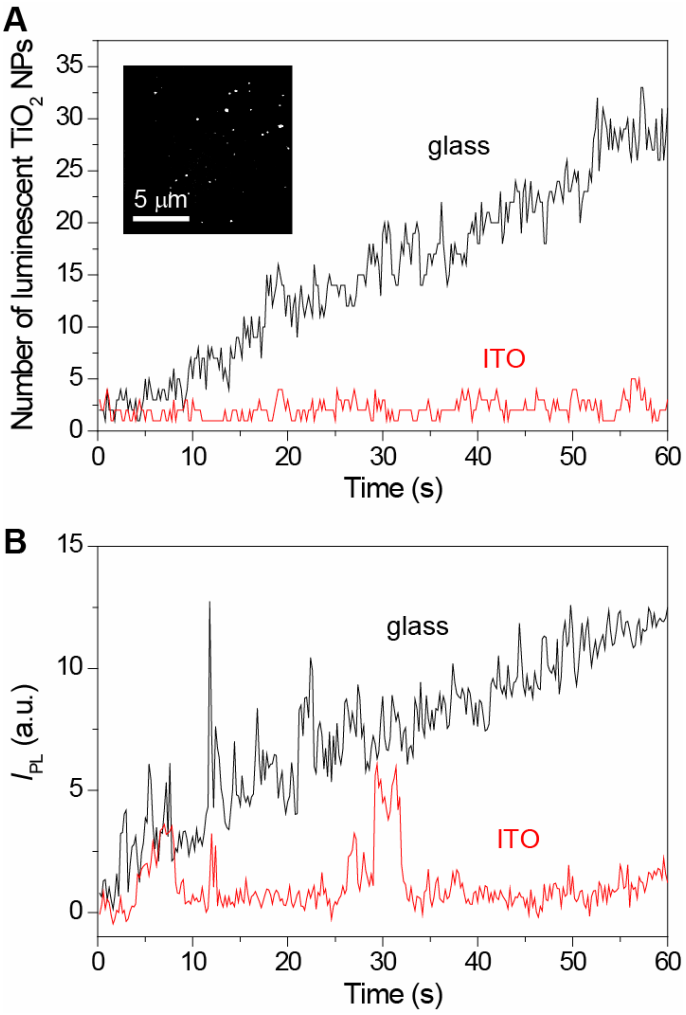

Figure S10. Number of luminescent spots (A) and trajectories of PL intensity (B) observed for TiO_2 nanoparticles spin-coated on the bare and ITO-coated cover glasses. See ref S11 for sample preparations. The integration time per one frame was 200 ms. Inset of panel A shows the typical PL image observed for TiO_2 nanoparticles on the glass surface under the 405-nm laser irradiation in Ar.

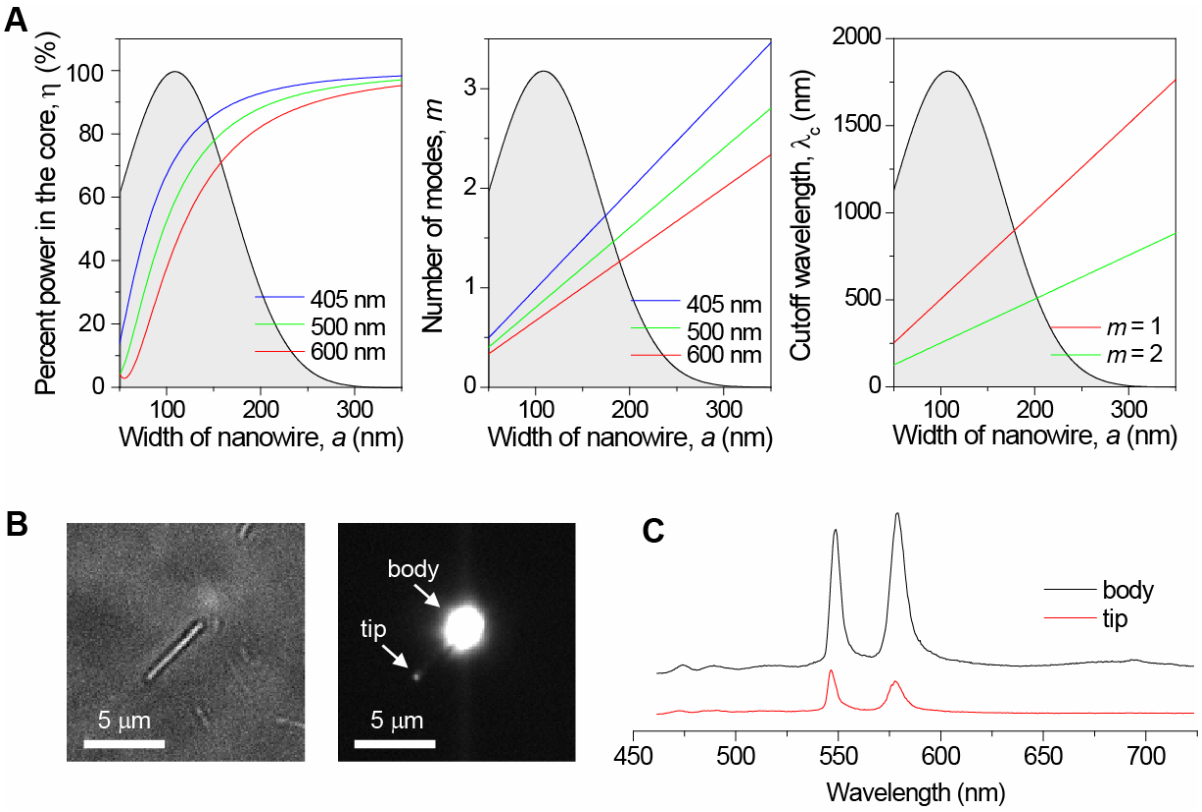

Figure S11. (A) Quantitative theoretical predictions of the waveguiding properties, such as the percent power in the core of the wire (η, left), the number of modes (m, middle), and the cutoff wavelength (λ_c, right). These parameters are respectively calculated by the following equations:

$$\eta = 1 - \left(2.405 \exp\left[-\frac{1}{V} \right] \right)^2 V^{-3}, \quad \text{S12} \tag{S1}$$

where a and n are the width and the refractive index of the fiber, respectively, and $V = \pi a / \lambda (n^2 - 1)^{1/2}$,

$$m = \frac{2a}{\lambda}(n - n_s), \quad \text{S13} \tag{S2}$$

where n_s is the refractive index of the substrate (n_s = 1.53 for cover glass),

$$\lambda_c = \frac{2na}{m}. \quad \text{S13} \tag{S3}$$

The gray-colored regions indicate the distribution of the wire width (a) determined by AFM analysis (see Figure S2). For example, the cutoff wavelength is λ_c = ca. 1000 nm for a = 200 nm. (B) Transmission (left) and emission (right) images captured in the same area. The body of the wire was locally irradiated with a mercury lamp (100 W, Ushio, USH-102D) through a pinhole (diameter is ca.1 μm on the cover glass). (C) Emission spectra observed at the body (black) and the tip (red) of the wire.

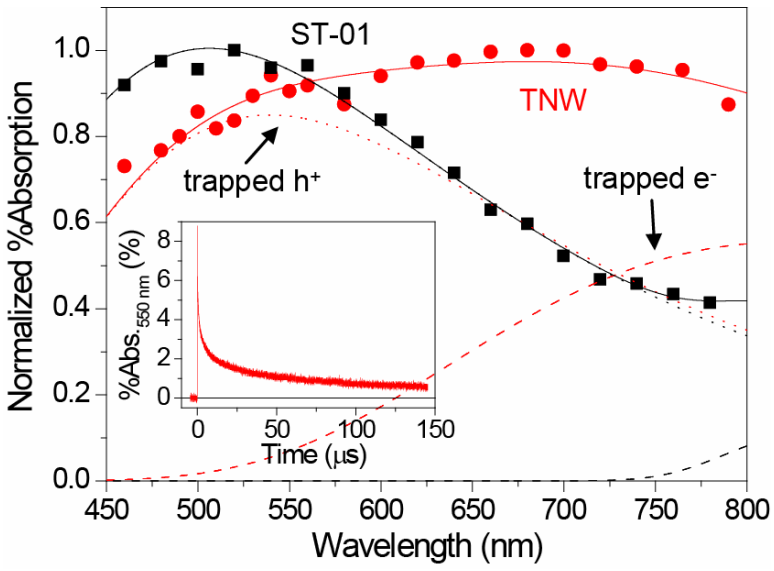

Figure S12. Time-resolved diffuse reflectance (TDR) spectra observed at 100 ns after the laser flash for TNWs and ST-01 in acetonitrile. Inset shows the time trace at 550 nm observed for the TNWs. The details of the experimental setup and spectral assignment are described in ref S14.

References

(S1) Fabregat-Santiago, F.; Garcia-Belmonte, G.; Bisquert, J.; Bogdanoff, P.; Zaban, A. *J. Electrochem. Soc.* **2003**, *150*, E293–E298.

(S2) Wang, G.; Wang, Q.; Lu, W.; Li, J. H. *J. Phys. Chem. B* **2006**, *110*, 22029–22034.

(S3) Wolcott, A.; Smith, W. A.; Kuykendall, T. R.; Zhao, Y.; Zhang, J. Z. *Small* **2008**, *5*, 104–111.

(S4) Armstrong, A. R.; Armstrong, G.; Canales, J.; Bruce, P. G. *Angew. Chem. Int. Ed.* **2004**, *43*, 2286–2288.

(S5) Kuno, M.; Fromm, D. P.; Hamann, H. F.; Gallagher, A.; Nesbitt, D. J. *J. Chem. Phys.* **2001**, *115*, 1028-1040.

(S6) Frantsuzov, P.; Kuno, M.; Jankó, B.; Marcus, R. A. *Nat. Phys.* **2008**, *4*, 519–522.

(S7) Protasenko, V. V.; Hull, K. L.; Kuno, M. *Adv. Mater.* **2005**, *17*, 2942–2949.

(S8) Glennon, J. J.; Tang, R.; Buhro, W. E.; Loomis, R. A. *Nano Lett.* **2007**, *7*, 3290–3295.

(S9) Peiro, A. M.; Colombo, C.; Doyle, G.; Nelson, J.; Mills, A.; Durrant, J. R. *J. Phys. Chem. B* **2006**, *110*, 23255–23263.

(S10) Knorr, F. J.; Mercado, C. C.; McHale, J. L. *J. Phys. Chem. C* **2008**, *112*, 12786–12794.

(S11) Tachikawa, T.; Ishigaki, T.; Li, J.-G.; Fujitsuka, M.; Majima, T. *Angew. Chem. Int. Ed.* **2008**, *47*, 5348–5352.

(S12) Johnson, J. C.; Yan, H.; Yang, P.; Saykally, R. J. *J. Phys. Chem. B* **2003**, *107*, 8816–8828.

(S13) Balzer, F.; Bordo, V. G.; Simonsen, A. C.; Rubahn, H.-G. *Phys. Rev. B* **2003**, *67*, 115408/1–115408/8.

(S14) Tachikawa, T.; Tojo, S.; Fujitsuka, M.; Sekino, T.; Majima, T. *J. Phys. Chem. B* **2006**, *110*, 14055–14059.